LABORATORY OF NUCLEAR MEDICINE AND RADIATION BIOLOGY

900 VETERAN AVENUE

UNIVERSITY OF CALIFORNIA, LOS ANGELES, CALIFORNIA 90024

AND DEPARTMENT OF RADIOLOGY

UCLA SCHOOL OF MEDICINE, LOS ANGELES, CALIFORNIA 90024

These studies were supported by Contract #EY-76-C-03-0012 between the U.S. Energy Research and Development Administration and the University of California.

Prepared for U.S. Energy Research
and Development Administration
under Contract #EY-76-C-03-0012

EMISSION COMPUTED TOMOGRAPHY: A NEW TECHNIQUE FOR THE QUANTITATIVE PHYSIOLOGIC STUDY OF BRAIN AND HEART IN VIVO

M.E. Phelps, Ph.D., Edward J. Hoffman, Ph.D., S.C. Huang, D.Sc., H.R. Schelbert, M.D., and D.E. Kuhl, M.D.

EMISSION COMPUTED TOMOGRAPHY:

A NEW TECHNIQUE FOR THE

QUANTITATIVE PHYSIOLOGIC STUDY OF BRAIN AND HEART IN VIVO

Michael E. Phelps, Ph.D., Edward J. Hoffman, Ph.D.,

Suen-Cheng Huang, D.Sc., Heinrich R. Schelbert, M.D.,

and David E. Kuhl, M.D.

Division of Nuclear Medicine
UCLA School of Medicine and
Laboratory of Nuclear Medicine and
Radiation Biology, University of
California, Los Angeles, California

This work was partially supported by DOE Contract EY-76-C-03-0012 GEN-12 and NIH Grant 7ROL-GM-24839-01.

DISCLAIMER

ABSTRACT

Emission computed tomography can provide a quantitative *IN VIVO* measurement of regional tissue radionuclide tracer concentrations. This facility when combined with physiologic models and radioactively labeled physiologic tracers that behave in a predictable manner allow measurement of a wide variety of physiologic variables. This integrated technique has been referred to by Phelps et al. as *Physiologic Tomogrpahy* (PT). A positron tomograph, the ECAT, has been well characterized in terms of analytical measurements of tissue radioactivity concentrations. The ECAT has been used to measure the rate constants for transport and metabolism of a glucose analog, (F-18)-2-fluoro-2-deoxyglucose in brain and heart. The compartmental model used in this work was developed by Huang, Phelps et al. This model and the measured rate constants have been incorporated into the ECAT operating system and used on a routine basis for measurements of regional metabolic rate for glucose in brain and heart. A model developed by Phelps et al. for measure of regional cerebral blood volume (rCBV) subsequent to single breath inhalation of ^{11}CO has also been incorporated into the ECAT. ^{11}CO is used both for study of rCBV and multiphase gated studies of cardiac blood pools. $^{13}NH_3$ is used with a unidirection transport model to examine capillary perfusion in brain and heart. Human studies are shown to exemplify each of the above approaches. In vivo investigation of biochemical and physiologic changes in normal and diseased states with PT provides a unique and fundamental capability. This approach can enrich our understanding and potentially allow characterization of disease at early stages where treatment and reversibility have a better perspective.

Tomographic techniques for minimizing or removing the superposition of information with depth have been the goal of a number of systems for producing an image of a section of the body in depth. In the past, most tomographic images in diagnostic radiology and nuclear medicine were produced by employing the principles of "focal plane" tomography, first described by Bocage in 1921. More recently, computerized mathematical techniques have been developed that allow exact or nearly exact reconstruction of tomographic sections of the body. This technique is referred to by the popular name of computerized tomography (CT). Although some of the first examples of computerized transaxial reconstruction tomography were demonstrated in nuclear medicine by Kuhl and co-workers (1-4), the successful development of the EMI (EMI Medical Ltd., Middlesex, England) x-ray transmission scanner by Hounsfield (5) has produced a rapid advancement in this technique in the past six years.

While the technique of CT is clearly applicable to nuclear medicine imaging, its clinical application has lagged far behind x-ray transmission CT (TCT). Although emission CT (ECT) is somewhat more difficult than TCT many of these technical problems have been or are now being solved (6).

ECT has a unique capability to quantitatively measure physiologic processes as compared to the more morphological or anatomical capabilities in TCT or ultrasound. This can be clearly appreciated from the fact that ECT can be combined with labeled body substrates and physiologic models to provide analytical measurements of metabolism, blood flow, blood volume, membrane transport, and other physiologic variables. This is achieved through the use of ECT to analytically measure tissue activity concentration _in vivo_. In this way ECT is an _in vivo_ analogy to _in vitro_ quantitative audioradiog-

raphy and tissue counting techniques which have been employed in a laboratory setting to study basic physiologic and pathophysiologic processes. This approach has been referred to as *physiologic tomography*, PT (7-8).

PT requires labeled compounds which trace physiologic processes in a known and predictable manner, and physiologic models which are appropriately formulated and validated to derive physiologic variables from ECT data. In order to effectively achieve this goal, PT requires an ECT system that is capable of performing truly quantitative or analytical measurements of tissue tracer concentrations and which has been well characterized in terms of spatial resolution, sensitivity and signal to noise ratios in the tomographic image.

This paper illustrates the capabilities of emission computed tomography and provides examples of physiologic tomography for the regional measurement of cerebral and myocardial metabolic rate for glucose, regional measurement of cerebral blood volume, gated cardiac blood pools and capillary perfusion in brain and heart. Studies on patients with stroke and myocardial ischemia are also presented.

METHODS

Reconstruction Algorithms

The basis of reconstruction tomography can be best illustrated with the example of transaxial CT (Fig. 1). Data are obtained from linear scans at discrete angles (or any equivalent scheme) around a cross-section of interest. These data are then processed in one of a number of mathematical algorithms to solve for the unknown cross-sectional structure. The mathematical approach is to reduce the 3-dimensional problem to one of two dimensions (2-D) by first assuming that the cross-section has no thickness (i.e., a 2-D plane). This 2-D problem is then partitioned into a linear series of 1-D

linear problems. For example, each datum point or detector reading, Y, in a linear scan is assumed to represent a linear equation of the form:

$$Y = A_1 + A_2 + \cdots + A_i$$

where A_1 through A_i are the unknown amounts of activity along the line-of view of the detector (Fig. 1). A linear set of these equations is generated during each linear scan. After sufficient data are collected in the linear and angular direction (9-11), a cross-sectional image can be unambiguously reconstructed. This formulation of the problem is the same for both x-ray and emission CT. However, there are a number of assumptions in the reconstruction algorithm that pose additional problems in ECT. For example, the assumption that each detector reading (Y in Eq. 1) is equal to the linear sum of activity in each picture element across a well defined line at each detector position (Fig. 1) neglects the fact that the photons emitted from the activity in the tissues are decreased in number to varying degrees by photon attenuation. Thus, photon attenuation represents another set of unknowns that must be solved or corrected for before the image can be reconstructed with conventional tomographic algorithms. Methods for compensating or correcting for photon attenuation have been developed and are discussed elsewhere (6, 12,13). Thus, the emission data are collected, corrected for photon attenuation and then mathematically reconstructed to form the final image of the cross-sectional distribution of tissue activity concentration (Fig. 2).

Present reconstruction algorithms can be separated into two categories: algebraic techniques, which generally use iterative schemes and fourier techniques which use fourier series, fourier transforms or convolution techniques. These techniques have been reviewed in several publications (9, 10, 11,

14). The most common reconstruction algorithm and that used in the system described in this work is convolution or linear superposition of filtered back projections.

A number of other physical factors and requirements of emission computed tomography are discussed elsewhere (6, 10-15).

Positron Imaging System

The tomograph used in this work is the ECAT (Fig. 3). This system is a positron tomograph which was jointly developed by Phelps and Hoffman (15) with ORTEC, Inc.* The ECAT is specifically designed for positron imaging and employs an electronic form of collimation in which the two 511 keV photons that are simultaneously emitted at 180° in positron decay are detected in opposing detectors with the aid of a coincidence circuit. This type of electronic collimation is referred to as annihilation coincidence detection, ACD (12) and avoids the lead collimators typically employed in nuclear medicine. ACD provides high spatial resolution, resolution and sensitivity which are depth independent and high geometric efficiency when multiple coincidence fan beam geometries are employed (12, 15-18). This type of multiple coincidence fan beam geometry is illustrated in the schematic representation of the ECAT (Fig. 4).

The ECAT consists of a hexagonal array of sixty-six 3.8 x 7.5 cm NaI detectors in which all detectors on opposing banks are connected in multiple coincidence. Linear (4 cm distance in discrete steps that are multiples of submultiples of 5.7 mm) scans at discrete angles (multiples or submultiples of 2.5°) are carried through a total angle of 60°. The data then sorted, corrected for photon attenuation and reconstructed with a convolution-based algorithm with an on-line PDP 11/45 minicomputer. The collected data are stored on

* Life Sciences Div., ORTEC, Inc., Oak Ridge, Tennessee

hard discs with final patient images stored on floppy discs. The images are displayed with the memory-buffered video display system in a 100 x 100 or 200 x 200 format with 64 grey levels or color. The patient is placed on a bed that can be moved up and down and in the axial direction either manually or under automatic control of the on-line computer so that the complete study can be carried out automatically by direct computer control. This system was designed as a high-contrast, high-efficiency, high-resolution, quantitative, fast scanning single-slice system representing an improved and optimized version of the PET III system originally developed by Phelps, Hoffman, Ter-Pogossian and co-workers (16, 17).

The ECAT is a whole body imaging system that can perform 3-dimensional tomographic studies and also 2-dimensional (2-D) imaging. The three opposing pairs of detector banks (Fig. 4) provide three simultaneous views of the patient in the 2-D mode (images at 0° and $\pm$ 60° oblique angles). Multiple tomographic cross-sections are obtained for a complete organ study in a serial fashion. Typically, a 2-D image of the patient is first performed and displayed in real time. The technician then selects the area to be studied tomographically by a joy stick on the console, enters the required number of tomographic cross-sections and the scanning sequence is then carried out automatically under computer control (see Figs. 7 & 10). All of the operations of the system are entered by a simple question-answer format through the video terminal and initiated by pushbuttons on the console. Both the tomographic and 2-D images can be corrected for attenuation with either an external ring source of positron activity or an automatic geometric correction (12, 15-17).

Scan times are selectable from 10 seconds to multiple minutes per slice

in the transaxial mode. Resolution is selectable in both the transaxial and 2-D imaging mode from 9 to 18 mm. (15).

The system is calibrated in terms of absolute concentration units with a uniform cylindrical phantom of known radioactivity concentration (15). The system software of the ECAT allows the user to extract region of interest concentrations, window the images, histogram or profile the images and a variety of other post-processing capabilities.

Physiologic Models

In general, the modeling approach we have taken with PT is to employ the type of compartmental models used in autoradiography and also equilibrium or steady state models (7-8).

Cerebral Blood Volume Model: The model for cerebral blood volume (CBV) was initially developed by Phelps et al. (21) for x-ray fluorescence measurements and later applied by Kuhl et al (22) to ECT. This equilibrium model is given by:

$$CBV = \frac{(^{11}CO\text{-}RBC)_T}{(^{11}CO\text{-}RBC)B \times 0.85 \times d} \qquad (1)$$

where $(^{11}CO\text{-}RBC)_T$ and $(^{11}CO\text{-}RBC)_B$ are the cerebral tissue and venous blood concentration of ^{11}CO labeled red blood cells (RBC), 0.85 is a correction accounting for the difference between large vessel and cerebral hematocrit (21) and d is the density of cerebral tissue (1.04 gm/cc). The value in the numerator is determined directly with the tomograph. The term in the denominator is measured from a single venous blood sample with a well counter. The red blood cells are labled by a single breath inhalation of ^{11}CO gas.

Glucose Metabolism Model: Determination of metabolic rate for glucose with (F-18)-2-fluoro-2-deoxy-D-glucose (FDG) as a glucose analog is based

upon a modification of the autoradiographic model of Sokoloff et al. (19). Sokoloff et al. used (C-14)-2-deoxyglucose (DG) as a glucose tracer for the measurement of cerebral metabolic rate for glucose (CMRGlu). The Sokoloff et al. model (19) is a first order transport model with 3 compartments in which deoxyglucose is transported by the same facilitated mechanism as glucose, except that DG is trapped in the cell in the phosphorylated form of DG-6-PO_4 (Fig. 5). DG-6-PO_4 is not further metabolized due to the inhibition or blocking of the 2 deoxy form of glucose (19). The CMRGlu is given by (19):

$$\text{CMRGlu} = \frac{C_P\left[C_i^*(t) - k_1^* e^{-(k_2^* + k_3^*)T}\int_0^T C_P^*(t) e^{(k_2^* + k_3^*)t}\,dt\right]}{LC\left[\int_0^T C_P^*(t)dt - e^{-(k_2^* + k_3^*)T}\int_0^T C_P^*(t) e^{(k_2^* + k_3^*)t}\,dt\right]} \quad (2)$$

where C_P and $C_P^*(t)$ are the mean plasma capillary concentration of glucose and DG, $C_i^*(T)$ is the total DG and DG-6-PO_4 concentration in the tissue, at region i and time T. The k*s are the rate constants for DG transport and phosphorylization between the various compartments (Fig. 5). LC is the lumped constant and is a set of six constants which reflect the rate of phosphorylization, dephosphorylization and volumes of distribution of deoxyglucose to glucose. At steady state, LC is equal to the ratio of the arterial-venous extraction fraction of DG to glucose across the organ of interest. This model assumes that once DG is phosphorylated to DG-6-PO_4 by hexckinase, it is not cleared from the tissue during the time of study. Brain or heart, contain only low activity levels of phosphotase, the enzyme which hydrolyses DG-6-PO_4 → DG PO_4.

Our studies indicate that loss of FDG-6-PO_4, although not large, is significant depending upon the time after the injection. Thus, we have rigorously derived a form of the Sokoloff et al. (19) model which includes

a k^*_4 term allow for hydrolysis of FDG-6-PO_4 back to FDG which then competes between clearance to the blood (k_2^*) and rephosphorylization (k^*_3) to FDG-6-PO_4 (Fig. 5). The general form of this model for the measurement of the metabolic rate for glucose (MRGlu) is given by:

$$MRGlu = \frac{C_P\left[C_i(T)^* - \frac{k_1^*}{\alpha_2-\alpha_1}\left((k_4^* - \alpha_1)d^{-\alpha_1 t} + (\alpha_2 - k_4^*)e^{-\alpha_2 t}\right)\right] \textcircled{X} C_P^*(t)}{LC\left(\frac{k_2^* + k_3^*}{\alpha_2-\alpha_1}\right)\left(e^{-\alpha_1 t} - e^{-\alpha_2 t}\right) \textcircled{X} C_P^*(t)} \quad (3)$$

where $\alpha_1 = \frac{k_2^* + k_4^*}{k_2^* + k_3^* + k_4^*}$, $\alpha_2 = k_2^* + k_3^* + k_4^* - \alpha_1$ and $\textcircled{X}$ is the operation of convolution.

We have measured the rate constants and the lump constant for both brain and heart. These rate constants along with the model have been directly incorporated into the software of the tomograph.

A simplified form of the model for the calculation of either the cerebral or myocardial metabolic rate for glucose (MRGlu) is given by:

$$MRGlu = \frac{\text{Plasma Glucose}}{\text{Lumped Constant}} \frac{(\text{Total of } ^{18}F \text{ in tissue} - \text{Free FDG in Tissue i,T}}{(\text{Total FDG delivered to the tissue})} \quad (4)$$

The total ^{18}F concentration in tissue at region i and time T is measured with the tomograph, the free FDG concentration in region i of the tissue is calculated from the rate constants and the measured plasma FDG concentration of time T, the total FDG delivered to the tissue is the area under the plasma concentration curve. We have shown (8) that all the blood values can be determined from venous blood from a resting arm without loss of accuracy compard to the use of arterial valves as employed by Sokoloff, et al. (19) or Reivich, et al. (20).

Capillary Perfusion: $^{13}NH_3$ injected as an intravenous bolus is presently used as a relative indicator of capillary perfusion (blood flow per gm of perfused tissue). The model for this approach as originally proposed by Phelps, et al. (23, 24) is based upon a unidirectional transport extraction of $^{13}NH_3$ from blood into tissue with fixation by metabolic trapping of $^{13}NH_3$ in the large amino acid pools of brain and heart. Schelbert et al. (25) have shown a linear relationship between tissue $^{13}NH_3$ concentration with myocardial blood flow over the range of zero to about 300cc/min/100gms. Above this flow range the $^{13}NH_3$ tissue concentration still increases but the response becomes nonlinear. Phelps, et al. have shown good agreement between the known distribution of cerebral blood flow and the distribution of $^{13}NH_3$ tissue concentration in the brain of human subjects (23, 24) in vivo and between $^{13}NH_3$ tissue concentration and flow measured with microspheres in dogs (unpublished work). The assumptions and requirements of this approach are disucssed in detail elsewhere (23-25).

RESULTS

The left-hand side of Fig 6 shows a 2-dimensional image of the distribution of blood in the human body taken with the ECAT subsequent to a single breath inhalation of ^{11}CO. Although this 2-dimensional image shows the overall distribution of blood it is limited in terms of the detailed distribution in any given organ. The tomographic images of the cross-sectional distribution at various levels through the brain shown on the right side of Fig. 6 illustrate the detail with which tomography can delineate the internal blood distribution of the brain. By using the model in Eq. 1 the tomograph provides images of cerebral blood volume in units of cc's of blood per gram of tissue on a regional basis.

Fig. 7 illustrates the tomographic capability to clearly delineate the individual chambers of the heart and large blood vessels that were not apparent on the 2-dimensional image (Fig. 6) because of superposition. In addition, the data collection of the tomograph can be gated by an EKG signal such that the tomographic images of the heart can be reconstructed for each phase of the cardiac cycle (Fig. 8). This allows one to calculate the mechanical work capability of each chamber of the heart by a simple and safe technique.

Fig. 9 is a human study of the cerebral metabolic rate for glucose using FDG. The 2-dimensional image of the head shown in the lower right hand corner of Fig. 9 illustrates the high concentration of FDG in the brain but the perception of the internal structures of the brain is limited. The cross-sectional tomographic images in the upper portion of Fig. 9 clearly illustrates the detailed delineation of the different substructures of the brain with ECT. Utilizing the model in Eq. 3 the images are converted to units of mg of glucose utilized per minute per gram of tissue. Thus one can extract the regional cellular metabolic rates in the human subject by a non-invasive technique.

Fig. 10 illustrates the study of myocardial glucose metabolism in the human subject. The 2-dimensional images on the right were taken to select levels to be examined tomographically. The 2-dimensional image at the top is taken with the ECAT in a transmission mode and is similar to a radiograph. The plus sign on the image illustrates where the operator has used the joy stick to select regions to be studied tomographically as illustrated at the far left hand side of Fig. 10 with transmission tomographic images of the thorax. The 2-dimensional image at bottom right side of Fig. 10 is the emission

image showing FDG localized primarily in the brain and heart. The plus sign on the 2-dimensional image again indicates where the operator has selected a starting point at the base of the heart for the tomographic examination. The tomographic emission images clearly show the glucose metabolism in the left (all levels) and right (top 2 levels) ventricle at levels that range from the base to the apex of the heart.

Fig. 11 illustrates a study of the patient with stroke in which $^{13}NH_3$ was used as a tracer to image the distribution of capillary blood flow. In addition, the patient was examined in terms of the cerebral metabolic rate for glucose with FDG and the integrity of the blood brain barrier with ^{68}Ga EDTA. The x-ray transmission tomographic study is shown on the far right of the figure and was read as normal even though the patient was symptomatic of an infarct in the right posterior portion of the occipital lobe of the brain. The ischemic infarct is clearly seen (as noted by the arrow) in both the blood flow and metabolism study and further delineated by the appearance of a blood brain barrier defect with ^{68}Ga EDTA (arrow).

Fig. 12 shows a patient with myocardial ischemia in the posterior wall of the left ventricle which is clearly seen in the $^{13}NH_3$ study (arrows). Note the close anatomical correspondence of the blood chambers (^{11}CO images) with the $^{13}NH_3$ images of the myocardium.

CONCLUSION

We have used the ECAT positron tomograph to investigate, characterize and validate the physiologic models and to apply them for the final measurement of physiologic variables in vivo. For example, the tomographic system was used to measure all of the rate constants in the model for the metabolic rate for glucose with FDG (Eq. 3) and then the model with the measured values

of the rate constants was incorporated into the operating system software of the ECAT to perform the in vivo measurements of metabolic rates for glucose. To carry out an actual study, the subject is injected intravenously with FDG, venous blood samples taken, and 30 to 40 minutes post injection are allowed to achieve steady state conditions before imaging is initiated. The blood data (plasma glucose concentration measured by the clinical lab and FDG plasma concentration measured in a well counter) are entered in the tomograph and the images are converted to units of glucose metabolic rate, (mg glucose utilized/min/gm tissue). Thus, as seen in Fig. 13, shortly after scanning, regional cerebral metabolic rate for glucose can be extracted with the region of interest capabilities of the ECAT. As region of interest is moved around to different locations in the image the metabolic rate, size of the region and standard deviation of variation within the region are updated in real time. This same approach is also employed in the measurement of myocardial metabolic rate for glucose. The system is set up in such a manner that the studies are now routinely carried out by nuclear medicine technicians.

The measurement of regional cerebral blood volume (rCBV) is accomplished with a simple single breath of ^{11}CO and about 3 venous blood samples. The blood concentration of ^{11}CO-carboxyhemoglobin is entered into the tomographic system and the rCBV values are then extracted in the same manner as discussed above for the glucose metabolic rate. ^{11}CO has also been used to image the ventricular chambers and large vessels of the heart. We have recently performed tomographic studies in which the multiple phase of the cardiac cycle are selected by EKG gating and stored in separate memory locations of the tomograph. Each phase of the cardiac cycle is then reconstructed (Fig. 8) and subsequently viewed in a cine format. This type of study not only provides

clear delineation of the ventricular chambers but also the calculation of the ejection fraction and stroke volume on a level to level and chamber to chamber basis. This technique allows one to observe akinesis associated with myocardial infarction and also to characterize the regional and global mechanical work capability of the heart.

After initial studies in normal subjects with FDG (8, 20, 26) the approach described in this paper was developed and has been applied to patients with i) epilepsy (27) ii) a wide variety of different types and changes in focal and diffuse cerebral ischemia (28) iii) cerebral tumors (15) and iv) ischemic heart disease (Fig. 10). This approach has also been used with $^{13}NH_3$ as a capillary perfusion tracer (25) to detect and characterize mild coronary artery stenosis down to a level of 47% stenosis (29).

ECT provides a non-invasive method to employ tracer methodology in a living subject for the measurement of physiologic variables with a spatial resolution and accuracy never before possible. *Physiologic Tomography* with short lived positron emitting radionuclides allows multiple studies and the study of time varying phenomena in a living subject without the perturbations and limitations imposed by destructive in vitro techniques. It also allows the study of human disorders in the human subject which avoid the difficulties or in some cases the impossibility (i.e. schizophrenia) of duplicating human disease in animals. The study and measure of in vivo biochemistry and physiology in normal and pathophysiologic states through *physiologic tomography* provides a unique and fundamental capability. This approach can enrich our understanding and potentially allow the characterization and detection of disease at early stages where treatment and reversibility of the disease have a better perspective.

FIGURE CAPTIONS

Figure 1. Schematic illustration of data collection format for transaxial emission computed tomography consisting of linear scans at discrete angles through 180° around the object. A_1, A_2, ...A_i, are the discrete amounts of activity within the detector field of view at each discrete step in the scans.

Figure 2. Data processing sequence of ECT. Emission data from linear scans ($f(x,y)$) are collected at discrete angles as shown in Fig. 1 to form the data set $m(r,\theta)$. These data are corrected for photon attenuation ($a(r,\theta)$) to produce $\hat{p}(r,\theta)$ which is then processed within a reconstruction algorithm to produce the final image in certesian coordinates ($\hat{f}(x,y)$).

Figure 3. The ECAT positron imaging system in Nuclear Medicine Clinic at UCLA.

Figure 4. Schematic illustration of ECAT. Example of multiple coincidence geometry is shown between one detector and all detectors of opposing bank. All detectors on opposing banks employ this type of coincidence logic to produce a total of 363 lines of coincidence response for the system (121 for each opposing pair of detector banks). In tomography all detector banks scan over a distance of 4 cm, the gantry rotates a fixed angle (typically 5°), detector banks scan in the opposite direction and this sequence is repeated through a total angle of 60°. The subject is automatically moved to the next position by computer control of the bed and the sequence is repeated in the opposite direction. In 2-dimensional (2-D) imaging the patient is moved through the tomograph in the axial direction as the detector

banks scan back and forth (no angular scanning is performed). The 3 opposing detector banks provide 3 simultaneous 2-D images of subject (0° and ± 60° oblique views).

Figure 5. Schematic illustration of compartmental model for the labeled glucose analoge of deoxyglucose or fluorodeoxyglucose. The k_1* and k_2* are the forward and reverse transport rate constants across the capillary membrane; k_3* and k_4* are the hexokinase mediated phosphorylation of deoxyglucose and the phosphatase mediated hydrolysis of deoxyglucose-6-PO_4 back to deoxyglucose.

Figure 6. Blood volume images subsequent to single breath inhalation ^{11}CO. Left: two dimensional rectilinear scans of the whole body blood distribution with the anterior-posterior and ± 60° oblique views. Total scan time, 20 minutes: resolution 1.3 cm. Right: cross sectional images of the brain (cerebral blood volume) starting at 6 cm above the orbital meatus, OM, and moving left to right and top to bottom to 3 cm below the OM in 15 mm increments. Top is anterior and left side is at left of image. The major structures seen in the images are superior saggital sinus, straight sinus and high blood volume in regions of the sylvian fissure and basal ganglia, lateral sinus, left and right carotid arteries and cavernous sinuses, signoid sinuses and a high blood volume in the nasal area. Resolution of 9.5 mm. Anterior is at top and left side is at left (adapted from ref. 15).

Figure 7. Example of transmission and emission studies in both a two dimensional and tomographic format. Left: transmission scans of the thorax. Bottom:

3 minute 2-dimensional (2-D) images of the thorax showing use of joy stick (x is position of joy stick cursor) to select levels which are automatically scanned in the transmission ECT mode (shown above). Right: emission images of the thorax subsequent to single breath inhalation of 10 mCi of ^{11}CO. Bottom: shows 3 minute 2-D images illustrating the use of the joy stick (x) to select levels which are automatically scanned with emission ECT as shown above. Emission images from top to bottom and left to right are from top of heart in 15 mm steps towards apex. Abbreviations: RV and LV right and left ventricular chamber; RA and LA, right and left arterial chamber; OF, out flow tract; A, aorta, SV, superior venacava; PA, pulmonary artery; IVS, intraventricular septum; IVC, inferior vencava. Images are ungated, resolution was 1.3 cm and images contained from 600,000 to 3,000,000 counts per level (taken from ref. 15).

Figure 8. Example of four phase gated study of the heart chambers in normal human volunteer. Subjects blood was labeled with a single breath of ^{11}CO (10 mCi). LV and RV are left and right ventricular chambers. RA is right atrium and A is aorta. Note synchrony in constriction of left and right ventricle (diastolic to systolic) and asynchrony with right atrium. Left side is at right and anterior is at top of each image. A single cross section of the thorax is shown in example.

Figure 9. Study of cerebral metabolic rate for glucose in human volunteer with ^{18}F-2-fluoro-2-deoxyglucose (FDG). Images in bottom right hand corner are from 2-dimensional scan of the head and illustrate the high uptake in the brain and poor delineation of the internal structures with 2-dimension imaging

(AP and two 60° oblique views are shown). Images above and left are cross-sectional tomographic images. Images at left to right and top to bottom are from 9 cm above to level of orbital meatus. Anterior is top and left side is left. Note clear delineation of superficial cortex, subcortical white matter, internal grey nuclei in the region of the basal ganglia (left and right caudate thalamus etc.), visual cortex, cerebellar cortex, vermus and brain stem that were not visualized in the two dimensional image. The model in eq. 3 was used to convert the images to units of cerebral metabolic rate for glucose (mgs glucose utilized per min. per gm of tissue).

Figure 10. Example of a study of myocardial glucose metabolism in human volunteer with FDG. Right: image at top is a two-dimensional (2-D) image of the chest in transmission mode showing the silhouette of the heart in the lung fields. The cross on the image shows the selection of levels for the tomographic study in the transmission mode (far left). At the bottom are shown 2-D images in emission mode subsequent to injection of FDG. Left: transmission tomographic images of the thorax from base to apex of heart. These images are used for morphological identification and attenuation correction of the emission images. Center: emission tomographic images of myocardial metabolic rate for glucose. Images are also from base to apex of heart. Top two levels show the myocardial metabolic rate for glucose in left and right ventricle while the lower images mainly show metabolic rate for glucose in left ventricle. The histogram profiles at the right illustrate image contrast between myocardium and surrounding lung and liver tissue. Histograms are at positions of + signs on the tomographic images. Image contrast of left ventricle to lung and liver are about 20 and 10, respectively.

Figure 11. Selected images from a patient with a right occipital cerebral infarct. $^{13}NH_3$ and FDG studies show the perfusion and metabolic deficit (arrow) resulting from ischemic infarct. Ga-68 EDTA images show the break down in the capillary membrane (blood brain barrier defect; arrow). The activity in the periphery of the head in Ga-68 EDTA images is in the extra cerebral tissue which does not have a blood brain barrier and therefore, activity freely diffuses into the tissue. Note, that if $^{13}NH_3$ images are superimposed on Ga-68 EDTA images, the blood brain barrier deficit corresponds directly to perfusion defect. X-ray CT scans with and without radiographic contrast material were read as normal (shown on right; adapted from ref. 15).

Figure 12. Capillary perfusion ($^{13}NH_3$) and blood chamber (^{11}CO) images of a patient with myocardial ischemia in the posterior wall of the left ventricle (arrows). Also note the close anatomical correspondence of the blood chambers (^{11}CO images) and the ventricular myocardium ($^{13}NH_3$ images). $^{13}NH_3$ was injected intravenously and ^{11}CO was administered by a single breath inhalation.

Figure 13. Illustration of region of interest (ROI) extraction of cerebral metabolic rate for glucose (CMRGlu). Eq. 3 and the measured values of the rate constants are resident in the operating system software of the ECAT so that after entry of plasma values for glucose and FDG concentrations the joy stick can be used to select ROI for display of ROI area, CMRGlu and standard deviation of variation of CMRGlu in ROI. As ROI is moved around image these parameters are updated in real time.

REFERENCES

1. Kuhl, D.E., Edwards, R.Q.: Image separation radioisotope scanning. RADIOLOGY 80:653-662, 1963.

2. Kuhl, D.E., Edwards, R.Q.: Reorganizaing data from transverse section scans using digital processing. RADIOLOGY 91:975-983, 1968.

3. Kuhl, D.E., Edwards, R.Q., Ricci, A.R., et al.: Quantitative section scanning using orthonal tangent correction. J. NUCL MED 14:196-200, 1973.

4. Kuhl, D.E., Edwards, R.Q., Ricci, A.R., et al.: The MARK IV system for radionuclide computed tomography of the brain. RADIOLOGY 121:405-413, 1976.

5. Hounsfield, G.N.: Computerized transverse axial-scanning (tomography) Part I: Description of systems. Ambrose, J.: Part II: Clinical applications. BR J RADIOL 146:1016-1047, 1973.

6. Phelps, M.E.: Emission Computed Tomography. SEM NUCL MED 7: 337-365, 1977.

7. Phelps, M.E., Hoffman, E.J., Kuhl, D.E.: Physiologic tomography: A new approach to in vivo measure of metabolism and physiologic funciton. IN: MEDICAL RADIONUCLIDE IMAGING, Volume I, IAEA, Vienna, pp. 233-253, 1977.

8. Phelps, M.E., Hoffman, E.J., Huang, S.C., et al.: Positron tomography: "In vivo" audioradiographic approach to measurement of cerebral hemodynamics and metabolism. IN: CEREBRAL FUNCTION, METABOLISM AND CIRCULATION, Ingvar, D.H., Lassen, N.A., Eds. Copenhagen, Munksgaard, 1977, pp. 446-447.

9. Phelps, M.E., Hoffman, E.J., Gado, M. et al.: Computerized transaxial transmission reconstruction tomography. IN: NON-INVASIVE BRAIN IMAGING, COMPUTED TOMOGRAPHY AND RADIONUCLIDES. De Blanc, H., Sorenson, J., Eds. N.Y., Society of Nuclear Medicine, 1975, pp. 111-146.

10. Brooks, R.A., DeChiro, G.: Principles of computer assisted tomography (CAT) in radiographic and radioisotope imaging. PHYS MED BIOL 21:689-732, 1976.

11. Ter-Pogossian, M.M., Phelps, M.E., Brownell, G.L., et al.: RECONSTRUCTION TOMOGRAPHY IN DIAGNOSTIC RADIOLOGY IN NUCLEAR MEDICINE, University Park Press, Baltimore, 1977.

12. Phelps, M.E., Hoffman, E.J., Mullani, N.A., et al.: Application of annihilation coincidence detection to transaxial reconstruction tomography. J NUCL MED 16:210-224, 1975.

13. Budinger, T.F., Gullberg, C.T.: Transverse section reconstruction of gamma-ray emitting radionuclides in patients. IN: RECONSTRUCTION TOMOGRAPHY IN DIAGNOSTIC RADIOLOGY IN NUCLEAR MEDICINE. Ter Pogossian, M.M., Phelps, M.E., Brownell, G.E., et al., Eds. University Park Press, pp. 315-342, 1977.

14. Budinger, T., Gullberg, G.T.: 3-dimensional reconstruction in nuclear medicine by iteretive least-squares and fourier transform techniques. IEEE Med Sci NS 21: 2-20, 1974.

15. Phelps, M.E., Hoffman, E.J., Huang, S.C., et al.: ECAT: A new computerized tomographic imaging system for positron-emitting radiopharmaceuticals. J NUCL MED 19: 635-647, 1978.

16. Phelps, M.E., Hoffman, E.J., Mullani, N.A., et al.: Design considerations for a positron emission transaxial tomograph (PETT III). IEEE, NS-23; 516-522, 1976.

17. Hoffman, E.J., Phelps, M.E., Mullani, N., et al.: Design and performance characteristics of a whole body transaxial tomograph. J Nucl Med 17: 493-502, 1976.

18. Budinger, T.F., Derenzo, S.E., Gullberg, G.T., et al.: Emission computed axial tomography. J COMPT ASSIST TOMOGR 1: 31-45, 1977.

19. Sokoloff, L., Reivich, M., Kennedy, C., et al.: The (^{14}C) deoxyglucose method for the measurement of local cerebral glucose utilization: theory, procedure and normal values in the conscience and anesthesized albino rat. J Neuro Chem 28: 897-916, 1977.

20. Reivich, M., Kuhl, D., Wolf, A., et al.: The (^{18}F) fluorodeoxyglucose method for the measurement of local cerebral glucose utilization in man. Circ Res (in press).

21. Phelps, M.E., Grubb, R.L., Ter-Pogossian, M.M.: In vivo regional cerebral blood volume by x-ray fluorescents: validation of method. J Appl Physiol 35: 741-747, 1973.

22. Kuhl, D.E., Reivich, M., Alavi, A., et al.: Local cerebral blood volume determined by 3-dimensional reconstruction of radionuclide scan data. Circ Res 36: 610-619, 1975.

23. Phelps, M.E., Hoffman, E.J., Coleman, R.E., et al.: Tomographic images of blood pool and perfusion in brain and heart. J Nucl Med 17: 603-612, 1976.

24. Phelps, M.E., Hoffman, E.J., Raybaud, C.: Factors which affect cerebral uptake and retention of $^{13}NH_3$. Stroke 8: 694-702, 1977.

25. Schelbert, H.R., Phelps, M.E., Hoffman, E.J., et al.: Regional myocardial perfusion assessed by N-13 labeled ammonia and positron emission computerized axial tomography. A J Card (in press).

26. Kuhl, D.E., Hoffman, E.J., Phelps, M.E., et al.: Design and application of the MARK IV Scanning System for radionuclide computed tomography of the brain. IN: Medical Radionuclide Imaging, IAEA, Vienna, pp. 309-320, 1977.

27. Kuhl, D.E., Phleps, M.E., Engel, J., Jr., et al.: Relationship of local cerebral glucose utilization and relative perfusion in stroke and epilepsy: Determination by emission computed tomography of (F-18) fluorodeoxyglucose and (N-13) ammonia. J Compt Tomo (in press).

28. Kuhl, D.E., Phelps, M.E., Hoffman, E.J. et al.: Initial clinical experience with ^{18}F-2-deoxy-D-glucose for determination of local cerebral glucose utilization by emission computed tomography. IN: Cerebral Function, Metabolism and Circulation. Ingvar, D.H., Lass, N.A., (eds), Munksgaard, Copenhagen, PP. 192-193, 1977.

29. Gould, K.L., Schelbert, H.R., Phelps, M.E., et al.: Noninvasive assessment of coronary stenosis by myocardial perfusion imaging during pharmacologic coronary vasodilaiton. Detection of 47% diameter coronary stennosis with $^{13}NH_4$ and emission computerized transaxial tomography in intact dogs. Am J Cardiol (in press).

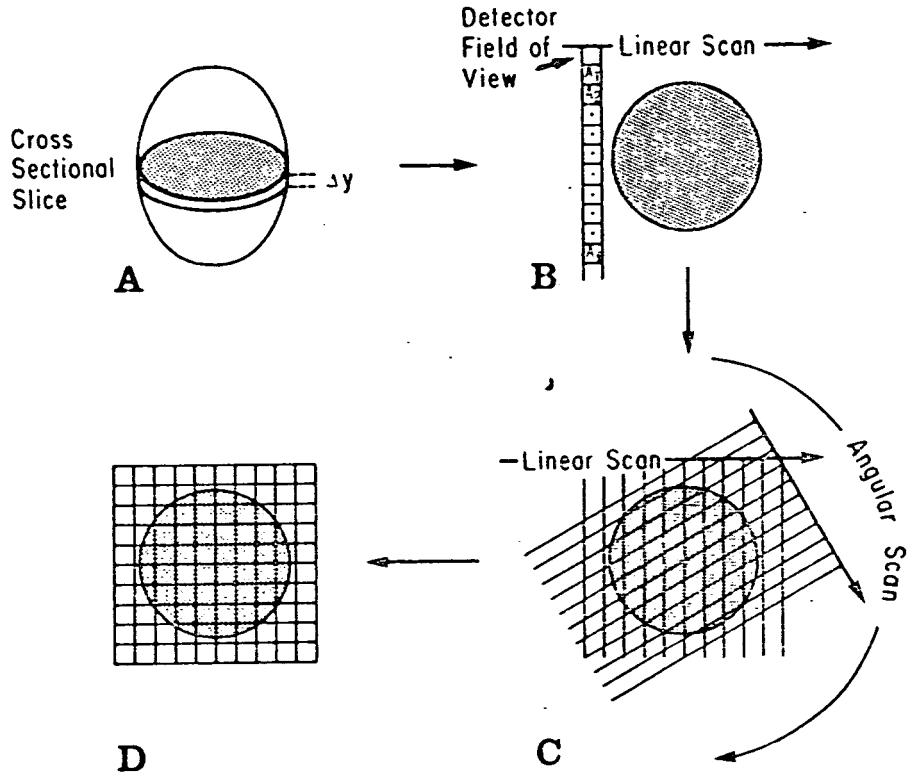

FIGURE 1

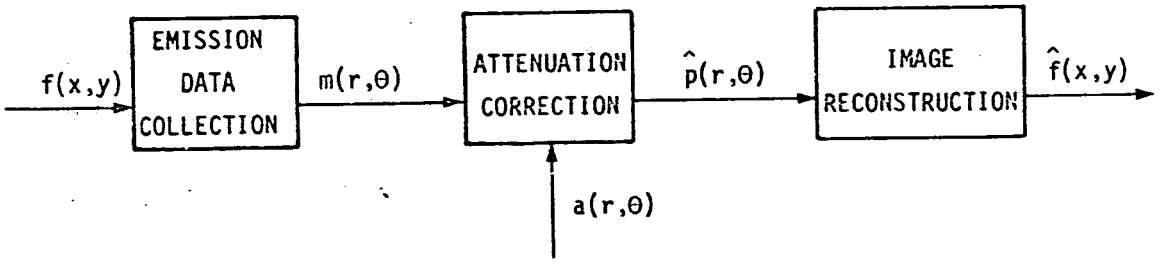

FIGURE 2

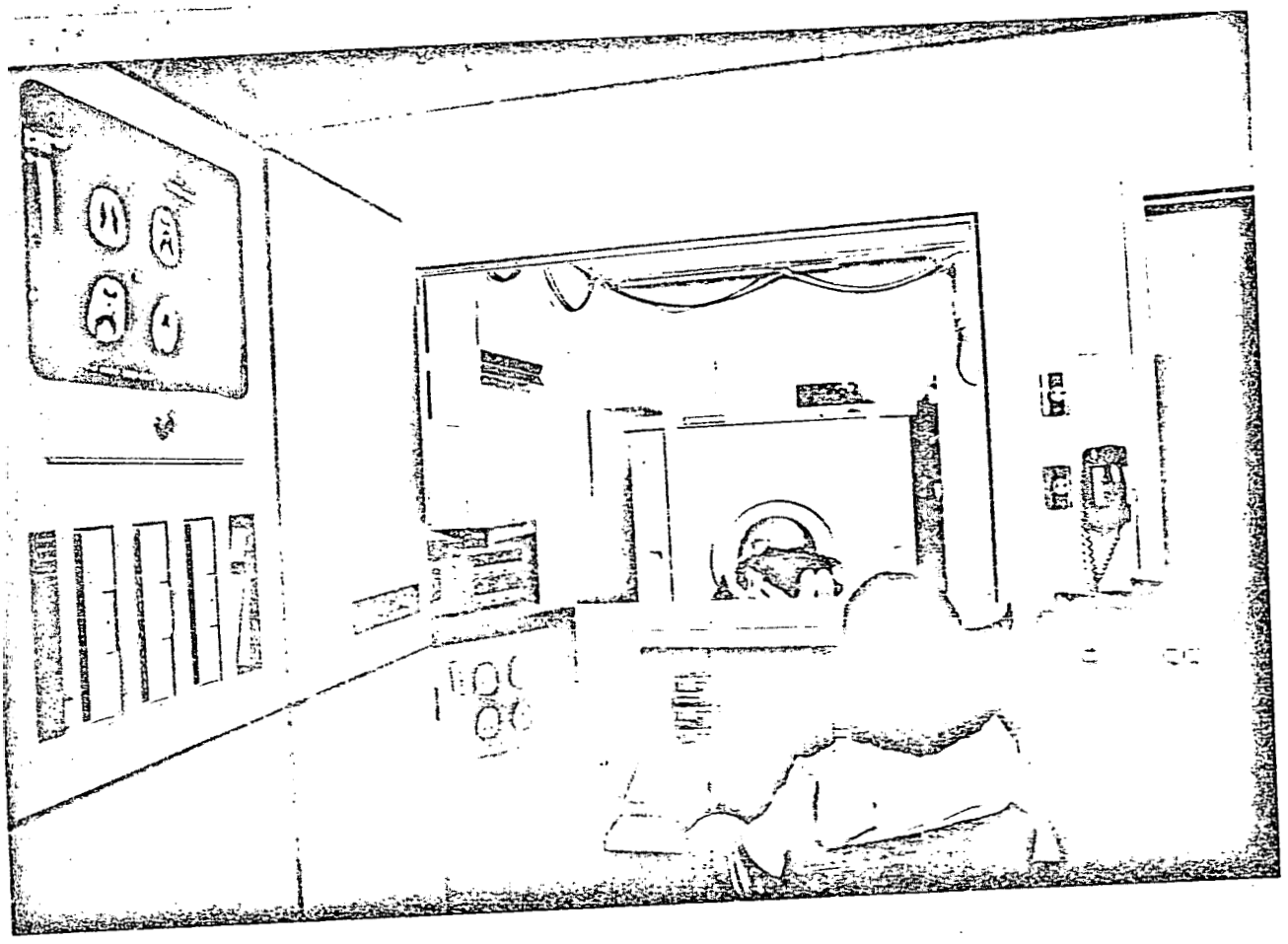

FIGURE 3

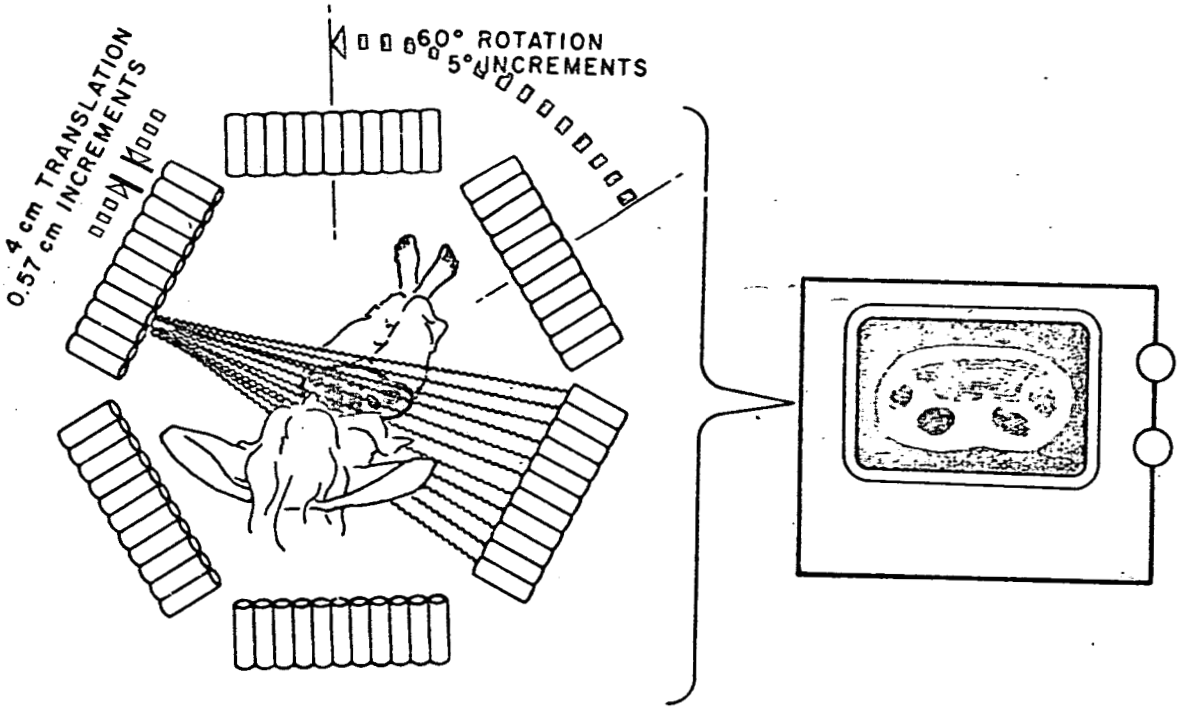

FIGURE 4

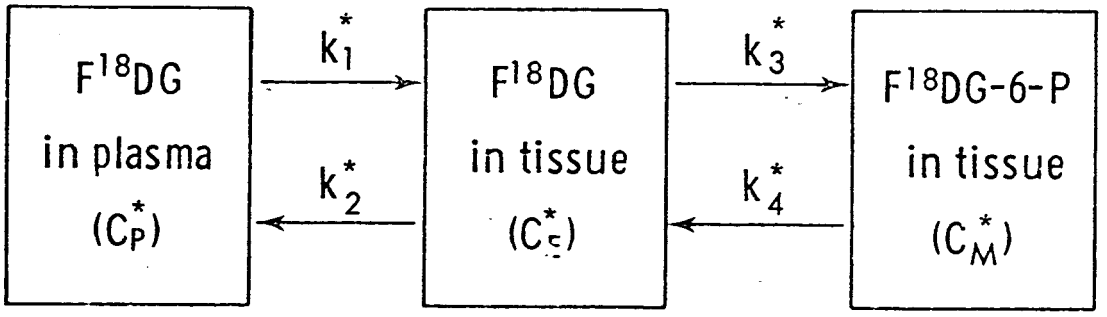

DIAGRAM OF THE THREE COMPARTMENTS IN FDG MODEL

FIGURE 5

^{11}CO

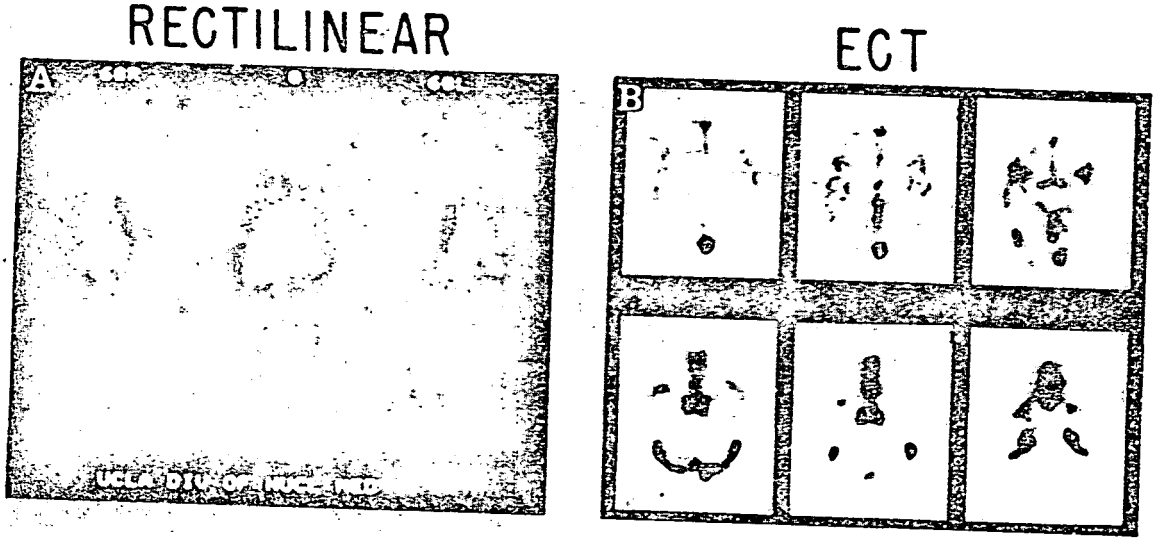

FIGURE 6

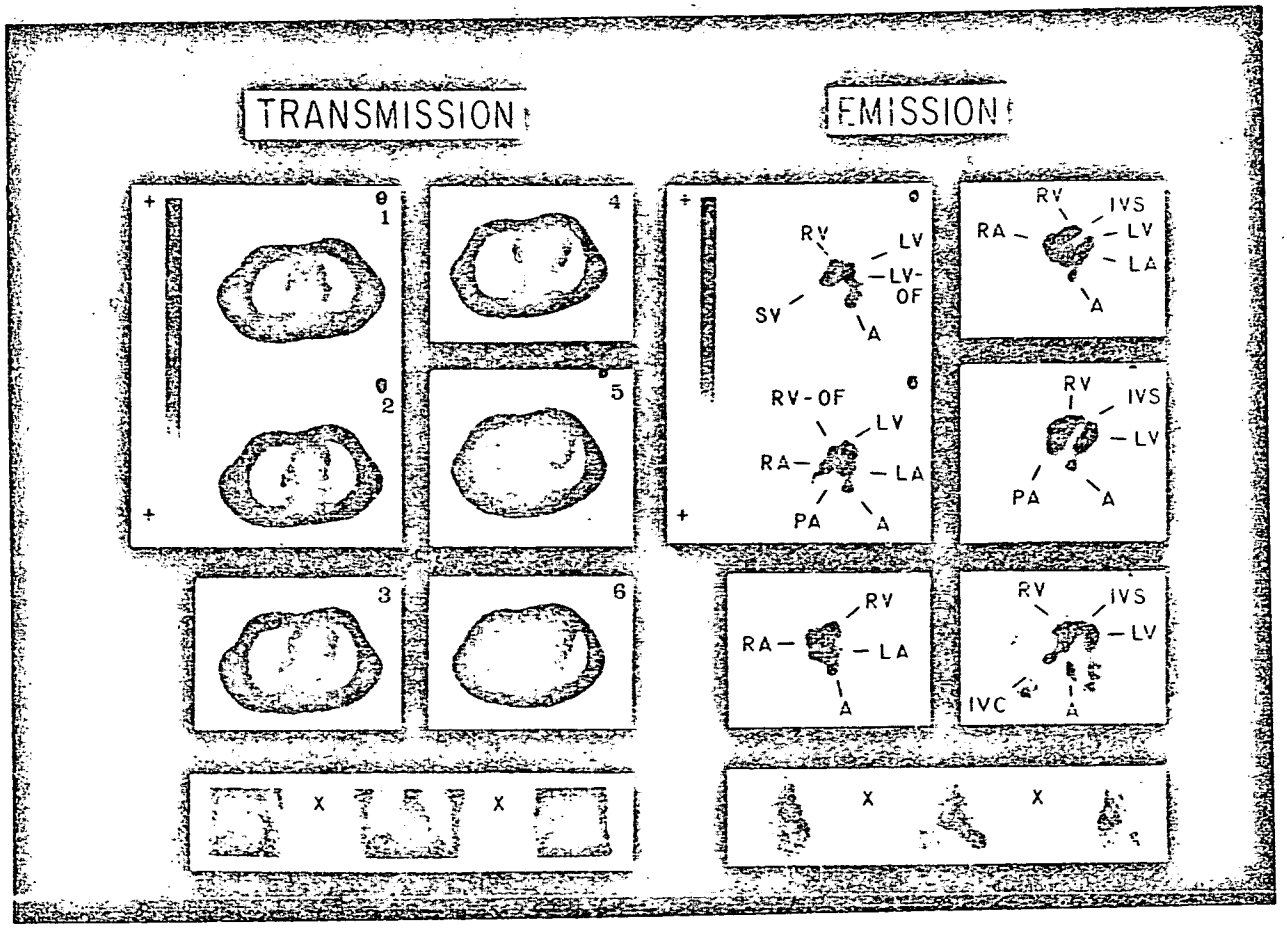

FIGURE 7

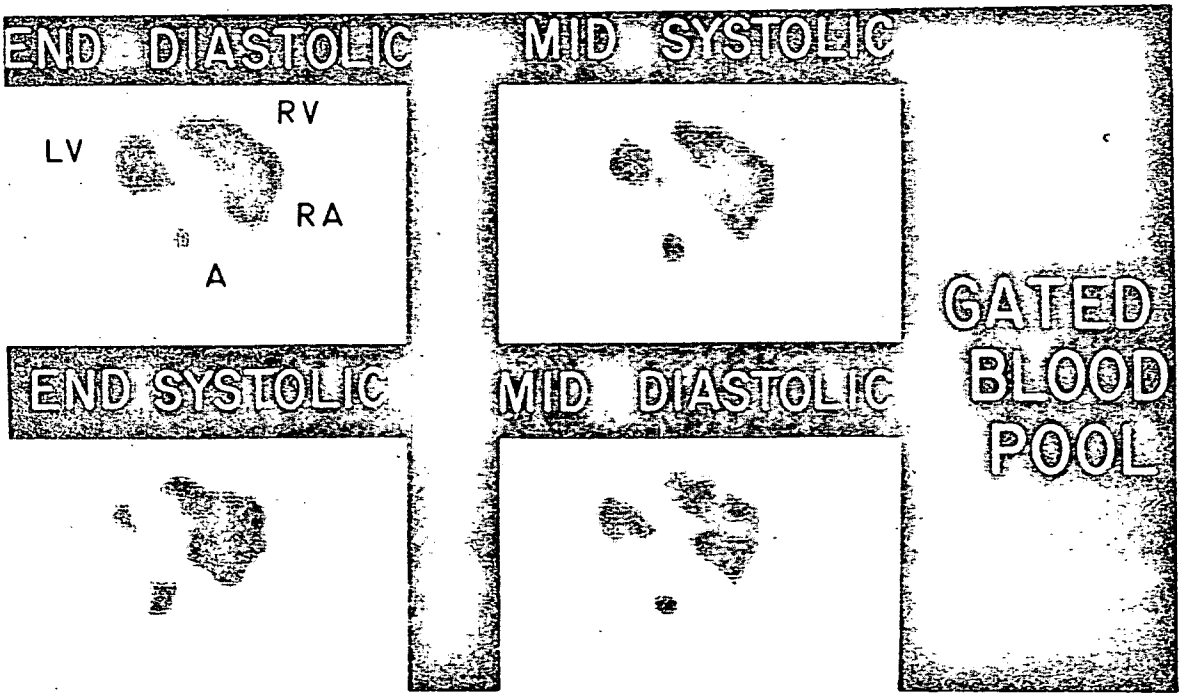

FIGURE 8

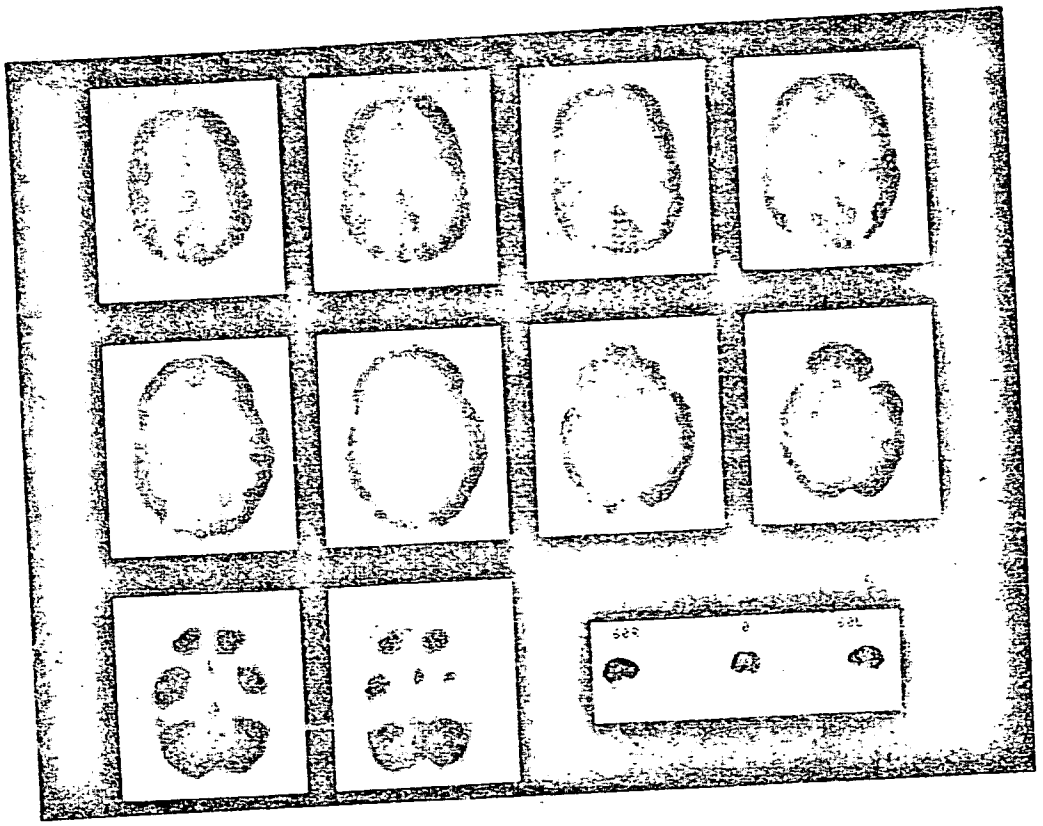

FIGURE 9

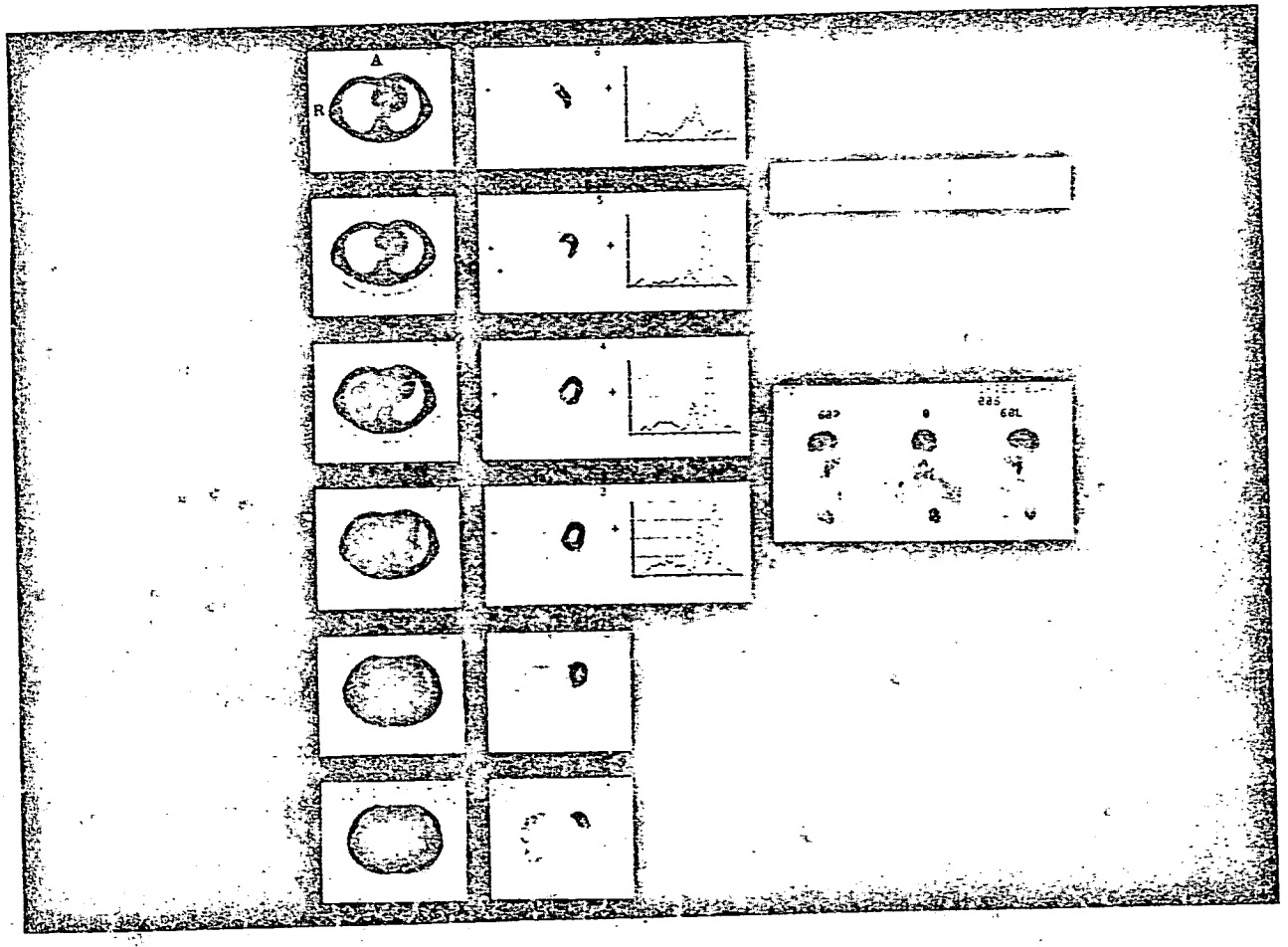

FIGURE 10

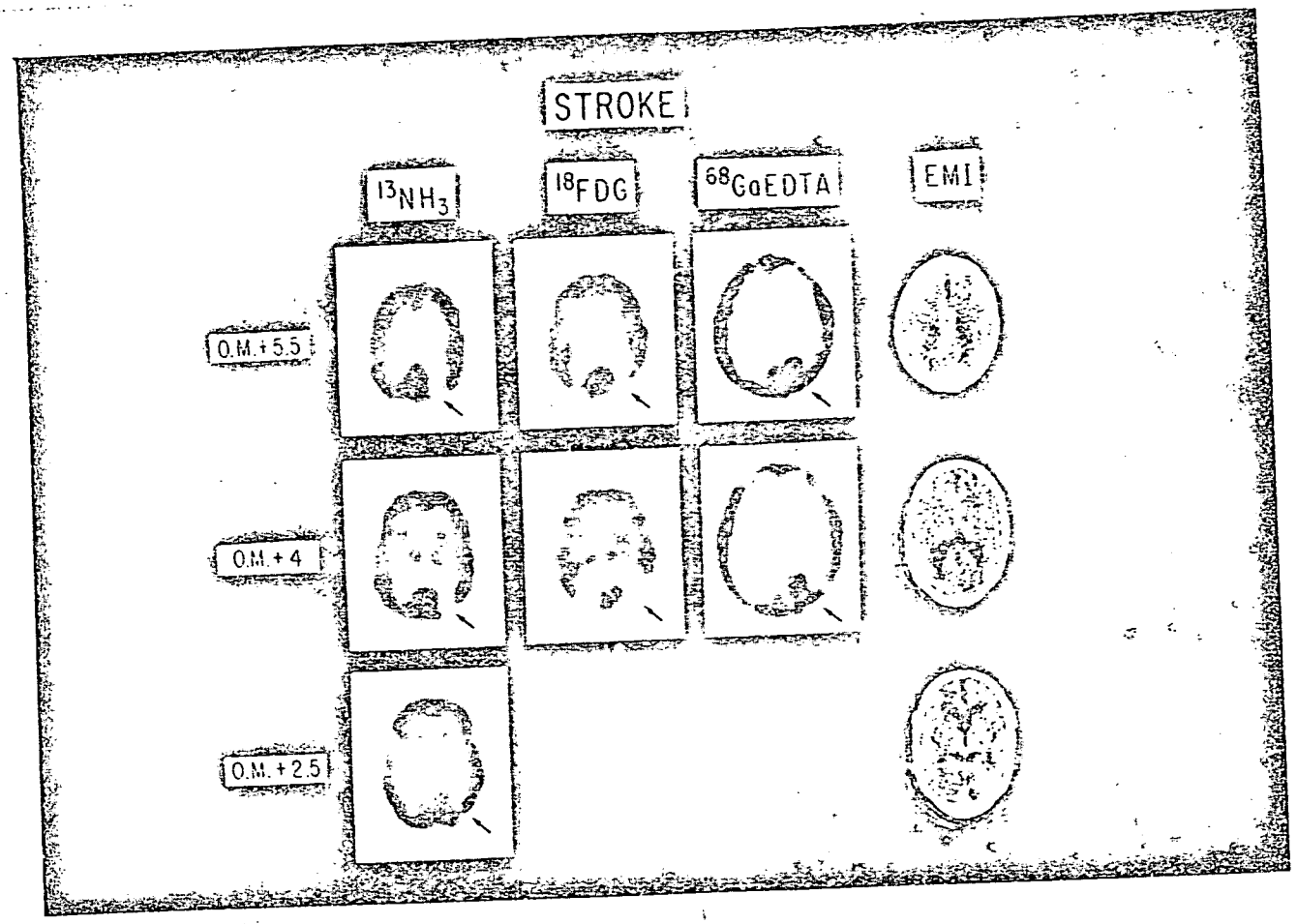

FIGURE 11

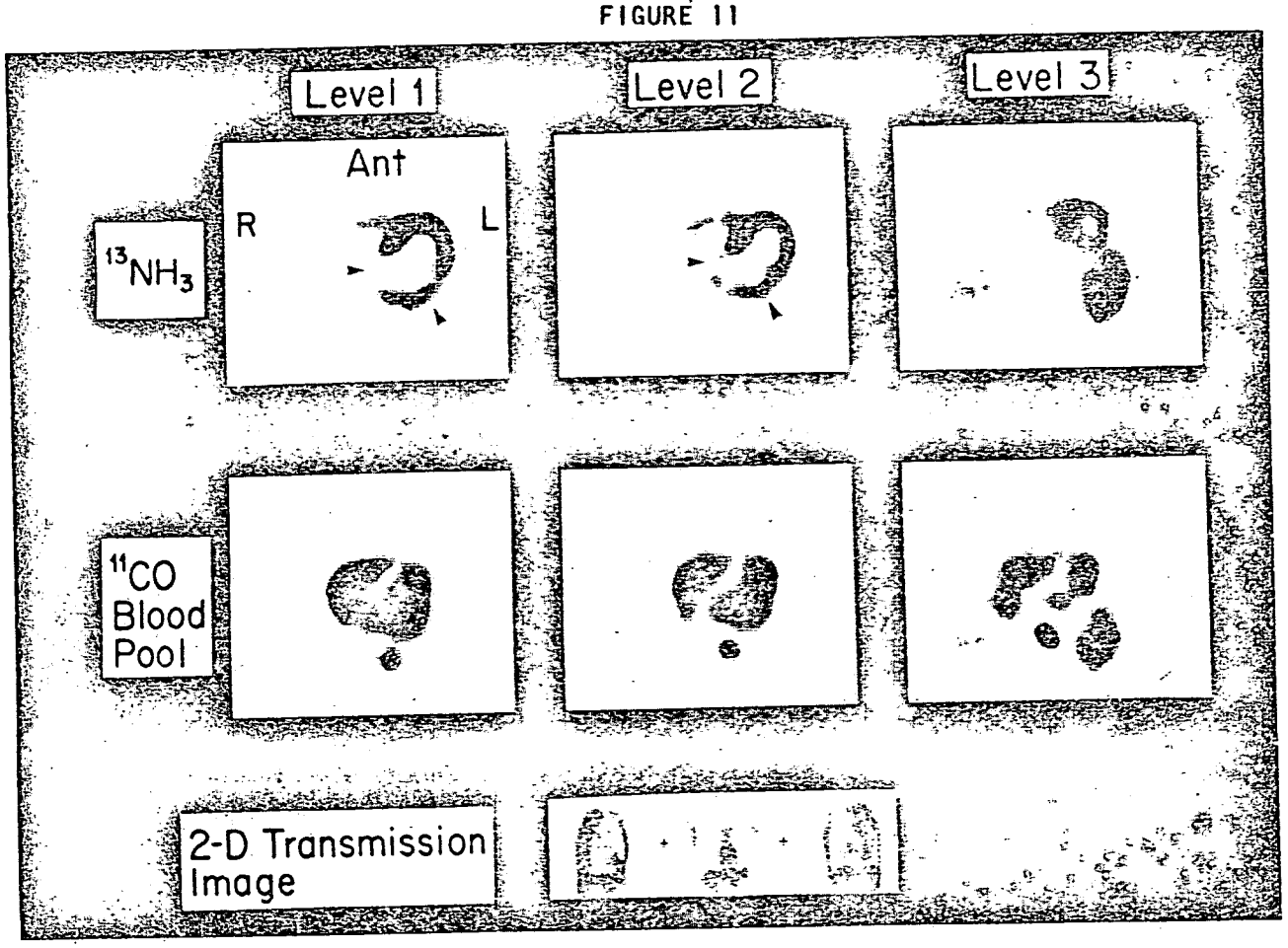

FIGURE 12

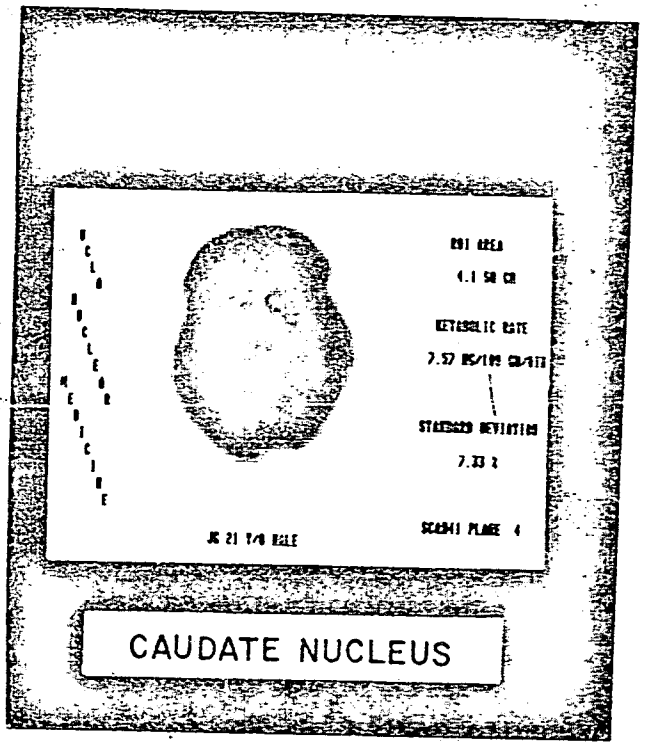

FIGURE 13